MNRAS 000, 1–12 (2018) Preprint 19 January 2018 Compiled using MNRAS LATEX style file v3.0

Another look at AM Herculis – radio-astrometric campaign with the e-EVN at 6 cm

M. P. Gawroński⋆, K. Goździewski, K. Katarzyński & G. Rycyk
Centre for Astronomy, Faculty of Physics, Astronomy and Informatics, Nicolaus Copernicus University, Grudziadzka 5, 87-100 Toruń, Poland

Accepted 2017 December 01. Received 2017 August 31; in original form 2017 February 10.

ABSTRACT
We conducted radio-interferometric observations of the well known binary cataclysmic system AM Herculis. This particular system is formed by the magnetic white dwarf (primary) and the red dwarf (secondary), and is the prototype of so-called polars. Our observations were conducted with the European VLBI Network (EVN) in the e-EVN mode at 5 GHz. We obtained six astrometric measurements spanning one year, which make it possible to update the annual parallax for this system with the best precision to date ($\pi = 11.29 \pm 0.08$ mas), equivalent to the distance of 88.6 ± 0.6 pc. The system was observed mostly in the quiescent phase (visual magnitude $m_v \sim 15.3$), when the radio emission was at the level of about 300 μJy. Our analysis suggests that the radio flux of AM Herculis is modulated with the orbital motion. Such specific properties of the radiation can be explained using the emission mechanism similar to the scenario proposed for V471 Tau and, in general, for RS CVn type stars. In this scenario the radio emission arises near the surface of the red dwarf, where the global magnetic field strength may reach a few kG. We argue that the quiescent radio emission distinguishes AM Herculis together with AR Ursae Majoris (the second known persistent radio polar) from other polars, as the systems with a magnetized secondary star.

Key words: star - astrometry: AM Her, cataclysmic variables - radio continuum: AM Her, cataclysmic variables - radiation mechanisms: AM Her

1 INTRODUCTION

Cataclysmic variable stars are a broad class of binary systems that consist a white dwarf (primary object) and mass transferring secondary star. The secondary component fills the Roche sphere and losses matter via L1 point. Among these objects we may distinguish a subclass of magnetic cataclysmic binary systems – called polars. In polars very strong magnetic field of the primary star (10 – 230 MG) prevents from the creation of accretion disks. The matter transferred from the secondary component must follow along magnetic field lines, and at the end falls into the magnetic pole/poles of the primary star. Such mass transfer leads to the formation of strong shocks nearby the surface of the white dwarf. As a result, the strong radiation is produced mainly by the bremsstrahlung and the electron cyclotron maser processes (Melrose & Dulk 1982; Dulk et al. 1983). An irregular variability in polars' luminosity on timescales from days to months is one of their main characteristics. As polars have no accretion disc, the changes in luminosity reflect variations in the mass transfer rate. The origin of the mass transfer rate instability is probably connected with the local magnetic activity of the secondary component. When active region on the secondary star is episodically drifting in the front of the inner Lagrangian point, the mass transfer is ceased due to the magnetic pressure of a large star-spot (Livio & Pringle 1994; Kafka & Honeycutt 2005). Alternatively, changes in the mass transfer rate could reflect variations in the size of active chromosphere, when the secondary star is not fulfilling the Roche lobe (Howell et al. 2000).

AM Herculis (hereafter AM Her) is one of the most intensively studied and intriguing magnetic cataclysmic binary system and the prototype of polars which are also named AM Herculis type stars. The irregular changes in AM Her brightness of $\Delta m_v \simeq 2$–3 mag (high and low states) are observed on timescales from weeks to months. Tapia (1977) suggested that AM Her contains a compact star with magnetic field of about 200 MG. After this AM Her became a frequent target in many observational campaigns, conducted at different wavelengths (e.g. Szkody 1978; Bunner 1978; Fabbiano et al. 1981), including also the radio bands (Melrose & Dulk 1982; Dulk et al. 1983; Bastian et al. 1985). Bailey et al. (1991) using infrared cyclotron features, estimated the white dwarf magnetic field strength to be $B \simeq 14.5$ MG, what was in a good agreement with previous results based on the Zeeman shifts of the photospheric absorption lines (e.g. Wickramasinghe & Martin 1985). The inclination of the system orbit $i \simeq 50°$ (Wickramasinghe et al. 1991; Davey & Smith 1996), and the period $P \simeq 3.094$ hr (e.g. Davey

⋆ E-mail:motylek@astro.umk.pl

Project code	Date [day]	[UT]	Epoch (JD-2450000)	Conv beam [mas]	[deg]	J1818+5017 $S^{\rm core}_{\rm 5GHz}$ [mJy]	J1809+5007 $S^{\rm core}_{\rm 5GHz}$ [mJy]	AM Her $S_{\rm 5GHz}$ [μJy]
EG069A	2012 Dec 5	07:06–09:47	6266.8521	10.0×6.0	-46	162±2	10±1	292±39
EG069B	2013 Feb 6	04:37–07:26	6329.7517	8.4×6.4	-64	142±1	11±1	371±34
EG069D	2013 May 2/3	21:28–00:20	6415.4535	9.9×6.2	-40	174±1	11±1	244±29
EG069Ea	2013 Sep 17	12:10–13:57	6553.0445	10.6×5.4	-51	166±2	9±1	178±32
EG069Eb	2013 Sep 17	21:11–23:56	6553.4369	10.5×5.5	56	167±1	13±1	347±31
EG069F	2013 Dec 3	16:38–19:05	6630.2444	9.9×5.2	55	146±1	11±1	297±35

Table 1. The observational log of our astrometric campaign.

Epoch (JD-2400000)	AM Her α (J2000)	$\Delta\alpha$ [mas]	δ (J2000)	$\Delta\delta$ [mas]	J1809+5007 α (J2000)	$\Delta\alpha$ [mas]	δ (J2000)	$\Delta\delta$ [mas]
47170.9996*	18 16 13.30576	120	49 52 04.3330	120	—	—	—	—
52929.5017*	18 16 13.23569	120	49 52 04.9571	120	—	—	—	—
56266.8521	18 16 13.192800	0.24	49 52 05.11172	0.23	18 09 15.069132	0.04	50 07 28.20070	0.04
56329.7517	18 16 13.193207	0.16	49 52 05.11928	0.15	18 09 15.069176	0.03	50 07 28.20091	0.02
56415.4535	18 16 13.192216	0.20	49 52 05.14021	0.21	18 09 15.069147	0.03	50 07 28.20094	0.03
56553.0445	18 16 13.188295	0.31	49 52 05.14569	0.26	18 09 15.069123	0.07	50 07 28.20143	0.06
56553.4369	18 16 13.188338	0.18	49 52 05.14614	0.16	18 09 15.069160	0.02	50 07 28.20137	0.02
56630.2444	18 16 13.188045	0.24	49 52 05.14066	0.20	18 09 15.069169	0.02	50 07 28.20141	0.02

Table 2. Astrometric position measurements of AM Her and J1809+5007. Their uncertainties are determined from the AIPS data fitting and do not include systematic effects. $*$ - positions based on archival VLA data (experiments AC206 and AM783).

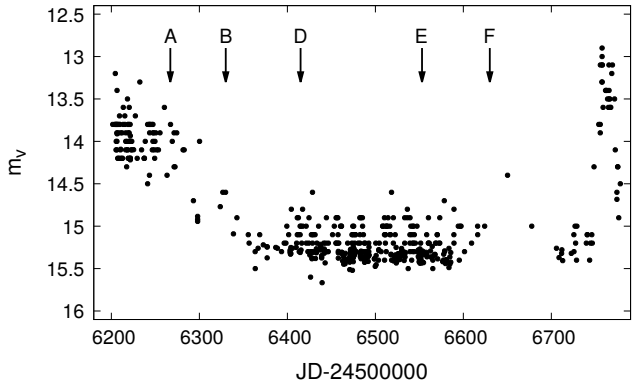

Figure 1. The optical light-curve of AM Her during our campaign (data from AAVSO). The epochs of the e-EVN observations presented in this paper are indicated by arrows.

& Smith 1996; Kafka et al. 2005) were also derived. The white dwarf mass estimations are in the range between $0.35-1.0\,M_\odot$ (e.g. Mouchet 1993; Gänsicke et al. 1998) with preferred value of $M_{wd} = 0.6-0.7\,M_\odot$ (Wu et al. 1995; Gänsicke et al. 1995). The secondary component is believed to be a $M4^+$–$M5^+$ type star (e.g. Gänsicke et al. 1995; Southwell et al. 1995) with the mass $M_s = 0.20-0.26\,M_\odot$ (Southwell et al. 1995).

The first detection the AM Her radio emission was achieved using the Very Large Array (VLA) at 4.9 GHz (Chanmugam & Dulk 1982). The measured flux density of AM Her was 0.67 ± 0.05 mJy, with no evidence of the circular polarization. Dulk et al. (1983) confirmed this detection, obtaining the flux density of 0.55±0.05 mJy and also specifying the upper limits to the flux density at 1.4 and 15 GHz (0.24 mJy and 1.14 mJy, respectively). In addition, these authors also discovered the radio outburst at 4.9 GHz with the maximum flux density of 9.7 ± 2.3 mJy, which was 100% RH circularly polarized. Dulk et al. (1983) also attributed the quiescent emission to gyrosynchrotron process, caused by mildly relativistic electrons with energies ~500 keV, trapped in the magnetosphere of the white dwarf. The electron-cyclotron maser located nearby the red dwarf, was proposed as a likely source of the radio outbursts. The same origin of radio flares was suggested by Melrose & Dulk (1982).

Young & Schneider (1979) derived the first distance estimation to AM Her d≃75 pc. Their finding was based on the analysis of various M-dwarf features in the optical spectrum. These authors additionally suggested, that secondary component in the system must be a M-dwarf with the spectral type between M4 and M5. In the next paper Young & Schneider (1981) presented another AM Her distance estimation ($d = 71 \pm 18$ pc), using the near-infrared CCD spectra and TiO bands analysis, which also revealed the presence of $M4^+$ companion. However, there is an indication that the red dwarf is illuminated by the white dwarf and the spectral type of the secondary component may be modulated with the orbital phase (Davey & Smith 1992). Dahn et al. (1982) determined the trigonometric parallax to 97 stellar systems, including AM Her ($d = 108^{+41}_{-28}$ pc). Gänsicke et al. (1995) used the so-called K-band surface-brightness method (Bailey 1981; Ramseyer 1994) and calculated the distance to AM Herculis as 91^{+18}_{-15} pc. The most recent distance estimation to the system of AM Her was made by Thorstensen (2003) with the use of the optical trigonometric parallax measurement with the 2.4 m Hiltner Telescope ($d = 79^{+8}_{-6}$ pc).

In this paper we present a new astrometric campaign with the European VLBI[1] Network (EVN) at 6 cm wavelength, which was

[1] VLBI – Very Large Baseline Interferometry

dedicated to the precise estimation of the AM Her annual parallax. This new value may be crucial for further modelling of physical processes in this system. The paper is structured as follows. In § 2 we describe observations and the data reduction. In § 3 we present a new astrometric model of AM Her. In § 4 we discuss observed AM Her radio properties and the orbital phase dependence of the radio emission. Finally, in § 5 we summarize our conclusions.

2 OBSERVATIONS AND DATA REDUCTION

The interferometric observations of AM Her at the 5 GHz band were carried out in 5 epochs, spread over 12 months from 2012 December 5 to 2013 December 3, using the EVN in the e-VLBI mode of observations, with use of the phase-referencing technique. The stations from Effelsberg, Jodrell Bank (MkII), Medicina, Noto, Onsala, Toruń, Yebes and Westerbork (phased array) participated in our observations (proposal code EG069). The data were recorded at the rate 1 Gb/s providing a total bandwidth of 128 MHz, divided into 8 base-band channels with a bandwidth of 16 MHz each. The fourth epoch was separated into two parts due to time allocation and both segments were treated during the reduction of data as separated epochs. The observation details of the all epochs are summarized in Tab.1.

Each observational epoch spanned ~3 hours covering scans on: AM Her, a bright bandpass calibrator, the phase-reference source (J1818+5017) and the secondary calibrator (J1809+5007). During the astrometric calculations we used J1818+5017 position taken from Radio Fundamental Catalog[2], version *rfc 2016d* (RA=$18^h18^m30^s.519224$, DEC=$50°17'19''.74353$, J2000.0). It means that we corrected the original position measurements based on radio maps by -0.13 mas in RA and -0.14 mas in DEC, respectively. These shifts compensate the difference between J1818+5017 positions in catalogs *rfc 2016d* and *rfc 2012b* (*rfc 2012b* was used during our observations and the correlation process).

J1809+5007 is a compact radio source selected from the Cosmic Lens All-Sky Survey[3] (e.g. Myers et al. 2003) placed in the proximity of AM Her (GB6J180913+500748, $F_{8.4\,\mathrm{GHz}}$ = 25.2 mJy). J1809+5007 was observed to examine the phase-referencing success. The three observed sources are separated on the sky plane as follows: AM Her & J1818+5017 by 0°.6, AM Her & J1809+5007 by 1°.2 and J1818+5017 & J1809+5007 by 1°.5 . The observations were made in 5 minute long cycles, 3.5 minutes for AM Her or J1809+5007, and 1.5 minute for the phase calibrator. The main loop of the observations contains five such cycles. The first cycle dedicated to J1809+5007 was followed by four cycles, which included integrations on AM Her. It should be mentioned that the first two epochs of the observations overlap with a decrease of the optical luminosity (blocks A & B). The rest of the measurements were recorded at the optical low-state of AM Her (blocks D, E & F). We show the AM Her optical light-curve during the campaign and the moments of our observations in Fig.1. The visual optical observations are taken from American Association of Variable Star Observers[4] database.

The whole data reduction process was carried out using standard NRAO package AIPS[5] procedures (e.g. Greisen 2003). The maps of the phase calibrator J1818+5017 were created with the self-calibration in the phase and the amplitude, and used as a model for final fringe-fitting. We applied the IMAGR task to produce the final total intensity images of all observed sources. During the mapping process the natural weighting was used. AM Her appears point-like at the radio maps, but for J1818+5017 we have detected a weak jet, pointed into east direction on all epochs. J1809+5007 also seems to be resolved at our maps with a hint of the jet suggestively directed into north-east.

A sample of radio maps obtained during our observations is showed on Fig.2. The radio fluxes and astrometric positions of all observed targets were then measured by fitting Gaussian models, using the AIPS task JMFIT. In the case of J1809+5007 and J1818+5017, we estimated only fluxes of the core, since the detailed modelling of these two sources is beyond the scope of this work. Moreover, these core fluxes completely dominate over the resolved structures. The flux variability was tracked using the task DFTPL with an averaging interval equal to the length of scans. Before application of the DFTPL task, we searched the area within the radius of 3″ around target's position for background sources and none was found. In a case of the background object detection, its model should be removed from *uv*-data, before radio flux estimation with DFTPL.

In order to expand the time span of the observations and to improve the proper motion estimation, we added two archival VLA observations at 8.4 GHz, made in BnA configuration (1988 Jan 10 and 2003 Oct 17, observational codes AC206 and AM783). The VLA observations were reduced with the AIPS package. Sources J1808+4542 and J1800+7828 were used as phase calibrators during AM783 and AC206, respectively. All positions collected in this paper are presented in Tab.2. The used VLA observations where short scans and the distant phase calibrators were used. Under the typical conditions of VLA observations, the astrometry accuracy of ~10 % of the restoring beam could be achieved (~0.″1 for AC206 and AM783). In the archival observations, the conditions are worse than during the standard observation, hence we made a crude estimation of the systematic error 0.″12 for VLA astrometry. It should be noted that VLA calibrators positions used during observations are taken from the different catalogs. This results in additional systematic effects in astrometry, which in general should be taken into account during calculations as calibrators position are relevant to the different global astrometric solutions. However, this effect is at the level of ~ 1 mas (the typical discrepancy between a given source position in different catalogs are sub-mas), and hence negligible in comparison to assumed by us systematic errors for VLA position measurements.

3 ASTROMETRIC MODEL AND AN ESTIMATE OF THE ABSOLUTE PARALLAX

Given the e-EVN measurements in the geocentric frame, we determine the parallax and the components of the proper motion through a canonical 5-element model for the ICRS astrometric place of an isolated target:

$$\vec{r}(t_i) = \vec{r}(t_0) + \vec{m}(t_i - t_0) - \pi \vec{E}_{\mathrm{B}}(t_i), \quad (1)$$

where $\vec{r}(t_i)$ is the geocentric position of the target at epoch t_i, relative to the position vector $\vec{r}(t_0)$ in a reference epoch t_0, $\vec{m}$ is the space motion vector, $\vec{E}_{\mathrm{B}}(t_i)$ is the barycentric position of the Earth at the observational epoch and π is the parallax of the radiation source. We note that due to a proximity of the phase-calibrators and the target, we skip local, differential perturbations, for instance due to the light deflection. We compute components of the vector mean motion

[2] astrogeo.org/rfc/
[3] www.jb.man.ac.uk/research/gravlens/class/class.html
[4] *AAVSO*, www.aavso.org
[5] www.aips.nrao.edu/index.shtml

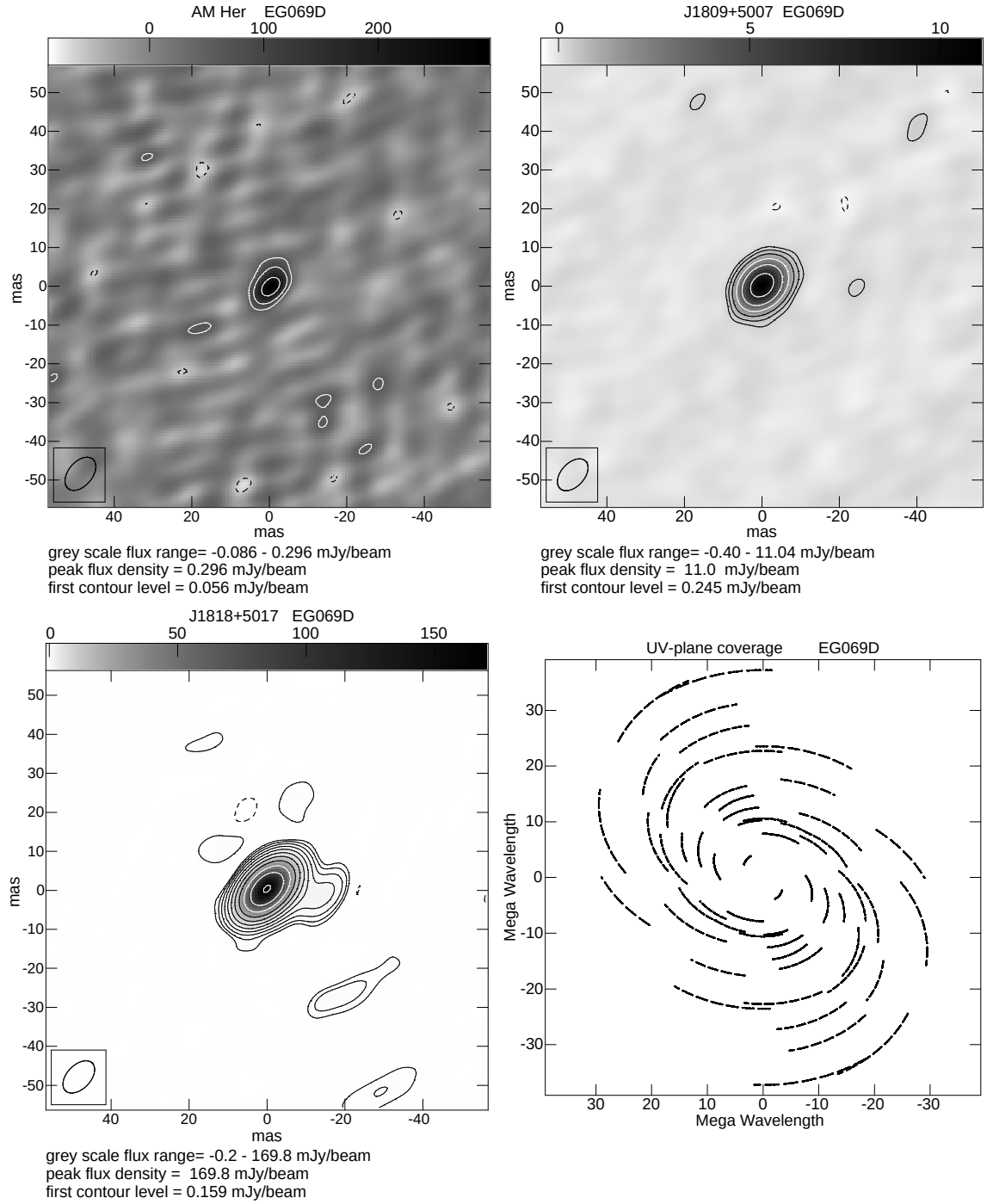

Figure 2. An example of the radio maps obtained from our campaign (*top left*: AM Her, *top right*: J1809+5007, *bottom left*: J1818+5017). The data were collected during the third epoch of the observations (EG069D). The successive contours show an increase of the flux density by a factor of 2, where the first contour corresponds to the detection limit of $\simeq 3\sigma$. The insets show the size of the restoring beam. The bottom right plot shows an example of typical AM Her observation *uv*-plane coverage, here also for EG069D part of the campaign.

$\vec{m} \equiv [m_x, m_y, m_z]$ by fixing the radial velocity $V_R = -12\,\mathrm{km\,s^{-1}}$ (Young & Schneider 1979).

The vector model in Eq. 1 may be parametrized through the target's ICRF coordinates (α_0, δ_0) at the initial epoch t_0, components (μ_α, μ_δ) of the proper motion at the epoch t_0, and the parallax factors (π_α, π_δ) projected onto the ICRF coordinates axes. To avoid correlations between the zero-epoch position and the proper motion components, we calculate the reference epoch t_0

$$t_0 = \frac{\sum_i^M t_i w_i}{\sum_i^M w_i} \equiv \mathrm{JD}\ 2456457.5, \quad w_i = \frac{1}{\sigma_i}, \tag{2}$$

which is the weighted mean of the observation epochs t_i, $i = 1\ldots, M$, and σ_i are formal uncertainties of the astrometric positions of the target derived from the radio maps. The barycentric

position of the Earth was determined in accord with the Solar system ephemeris JPL DE405 (Folkner et al. 2014).

We optimized the astrometric model with the same approach as presented in Gawroński et al. (2017). Uncertainties of the model parameters $\boldsymbol{\xi} = (\alpha_0, \delta_0, \mu_\alpha, \mu_\delta, \pi)$ depend on complex way on the residual phase in phase-referencing, sub-mas changes of the phase calibrator radio structures and the atmospheric zenith delay residuals. To account for such factors, the formal uncertainties are rescaled in quadrature, $\sigma_i^2 \rightarrow \sigma_i^2 + \sigma_f^2$, where σ_f is the so called error floor added as an additional free parameter to be optimized. To do so, we define the maximum likelihood function $\mathcal{L}$. For normally distributed uncertainties σ_i, we account for the error floor σ_f, defining $\mathcal{L}$ as follows

$$\log \mathcal{L} = -\frac{1}{2}\sum_{i,t}\frac{(\mathrm{O\text{-}C})_i^2}{{\sigma_i}^2 + \sigma_f^2} - \frac{1}{2}\sum_i \log({\sigma_i}^2 + \sigma_f^2) - M \log 2\pi, \quad (3)$$

where $(\mathrm{O\text{-}C})_{j,t}$ is the (O-C) deviation of the observed $\alpha(t_i)$ or $\delta(t_i)$ at epoch t_i from its astrometric ephemeris in Eq. 1, for $i = 1 \ldots, M$ where M is the total number of $\alpha(t_i)$ and $\delta(t_i)$ measurements. It makes it possible to determine the error floor σ_f in a self-consisted manner.

We analyse the $\log \mathcal{L}$ function in terms of the Bayesian inference. We sample the posterior probability distribution $\mathcal{P}(\boldsymbol{\xi}|\mathcal{D})$ of astrometric model parameters $\boldsymbol{\xi}$ in Eq. 1. Given the data set $\mathcal{D}$ of astrometric observations data-set (understood as α_i and δ_i components): $\mathcal{P}(\boldsymbol{\xi}|\mathcal{D}) \propto \mathcal{P}(\boldsymbol{\xi})\mathcal{P}(\mathcal{D}|\boldsymbol{\xi})$, where $\mathcal{P}(\boldsymbol{\xi})$ is the prior, and the sampling data distribution $\mathcal{P}(\mathcal{D}|\boldsymbol{\xi}) \equiv \log \mathcal{L}(\boldsymbol{\xi}, \mathcal{D})$. For all parameters, we define noninformative priors by constraining the model parameters, i.e., $\alpha_0 > 0\,\mathrm{hr}$, $\delta_0 > 0\,\mathrm{deg}$, $\mu_\alpha^*, \mu_\delta \in [-1000, 1000]$ mas yr^{-1}, $\pi > 0$ mas and $\sigma_f > 0$ mas.

We used the EMCEE package developed by Foreman-Mackey et al. (2013) to perform the posterior sampling with the Markov Chain Monte Carlo (MCMC) technique. In all experiments, we increased the MCMC chain lengths to up to 72,000 samples and 2240 random "walkers" selected initially in a small radius hyperball around a preliminary astrometric solution found with the simplex algorithm. The MCMC acceptance ratio was near 0.5 in all cases.

We performed a few fitting experiments for three sets of measurements (see Table 2). The first set comprises of all six EVN detections. The second set contains all EVN and VLA epochs. The third set comprises of a minimal number of four EVN epochs that make it possible to determine the absolute parallax. We optimized the 5-element model with and without the error floor. For the EVN data, we computed the astrometric parameters at the GAIA DR1 epoch JD 2457023.5, to have a direct link to the forthcoming GAIA catalogue (Lindegren et al. 2016).

The derived astrometric parameters for different data sets and epochs are displayed in Table 3. Since the MCMC posteriors look similar for all datasets, we illustrate only the astrometric model for six EVN epochs (see Tab. 2 and the left column in Table 3). The results are illustrated in Fig. 3 and Fig. 4 as one– and two–dimensional projections of the posterior probability distributions for astrometric model with and without accounting for the error floor correction, respectively. It may be compared with the posterior derived for a model with the error floor included (Fig. 4). The error floor parameter is in fact redundant for the AM Her e-EVN data, since its posterior probability has a maximum at $\sigma_f = 0$ mas, it is small and almost "flat" elsewhere with a median around 0.15 mas. Indeed, the 5-parameter astrometric model yields $\chi^2 \sim 1$, and including the additional parameter does not improve the astrometric fit.

In the best-fitting solution for all e-EVN data in Table 2, the AM Her parallax $\pi = 11.29 \pm 0.08$ mas, which is equivalent to the distance of $d = 88.6 \pm 0.6$ pc. This is formally the most accurate and absolute determination of the AM Her distance, as compared to previous estimates in (e.g. Gänsicke et al. 1995; Thorstensen 2003). This new estimate roughly agrees with the most recent determination based on the optical observations ($d = 79^{+8}_{-6}$ pc; Thorstensen 2003), yet our uncertainty is one order of magnitude smaller.

The top panel of Fig. 5 illustrates the synthetic paralactic motion of the target over-plotted with the original measurements as blue (grey-white) filled circles. In this scale the error-bars are smaller than the circle diameter. To best fitting model (red/dark grey curve) is over-plotted on 100 randomly sampled models from the posterior data (Fig. 3) for the time interval ±465 days w.r.t the first and last data epochs, respectively.

We also compared the inferred model positions with AM Her radio maps from our campaign, and in all cases they agree well. The residuals to the final astrometric model based on the EVN observations in Tab. 2 are illustrated in Fig. 6. Curiously, there is some systematic trend of the residuals apparent, however a sparse sampling makes it hardly possible to interpret the pattern of the residuals. Given the small error floor parameter, it has unlikely systematic meaning.

Given that the EVN observations are very expensive in terms of the human power and telescope time, we did also a simple experiment for estimating a minimal number of observations required to reliably determine the parallax of relatively distant, AM Her-like targets. We assume that observations with sub-mas level uncertainties are scheduled to cover the whole year time-window. We found that three observations are not sufficient to determine the parallax. With six (α, δ) datums, the astrometric model in Eq. 1 is closed, but we could not find any reliable solution using the MCMC optimization procedure. With four observations, the results are very similar to the parameters obtained for the whole EVN data set, both in terms of the numerical values (Table 3) and the posterior distribution.

Finally, we extended our e-EVN measurements with two archival VLA observations from the NRAO database[6]. The VLA data, back to 1988 and 2003, could improve the determination of the proper motion. For the same reason, we could use optical measurements in Thorstensen (2003), however, they are not available in source form and the reference paper reports large uncertainties $\sim 1''$. We also found an infra-red position from the 2MASS catalogue (Skrutskie et al. 2006), which has similarly substantial uncertainty of ~ 80 mas.

We added the VLA measurements aiming to improve the mean motion parameters, since the EVN data cover only one year. Unfortunately, the uncertainties are much larger for this set than for the e-EVN data, and the VLA measurements stand out from the model (the bottom panel in Fig. 5). Yet the spread of models randomly selected from the posterior, is quite limited for almost three decades interval. We found that the posterior distribution looks like the same as for the EVN data. We did not find any improvement of the mean motion parameters too, see Table 3.

4 PROPERTIES OF THE OBSERVED RADIO EMISSION

The radio emission traces particle acceleration and hence is a very useful probe of physical conditions in various astrophysical sys-

[6] science.nrao.edu/facilities/vlba/data-archive

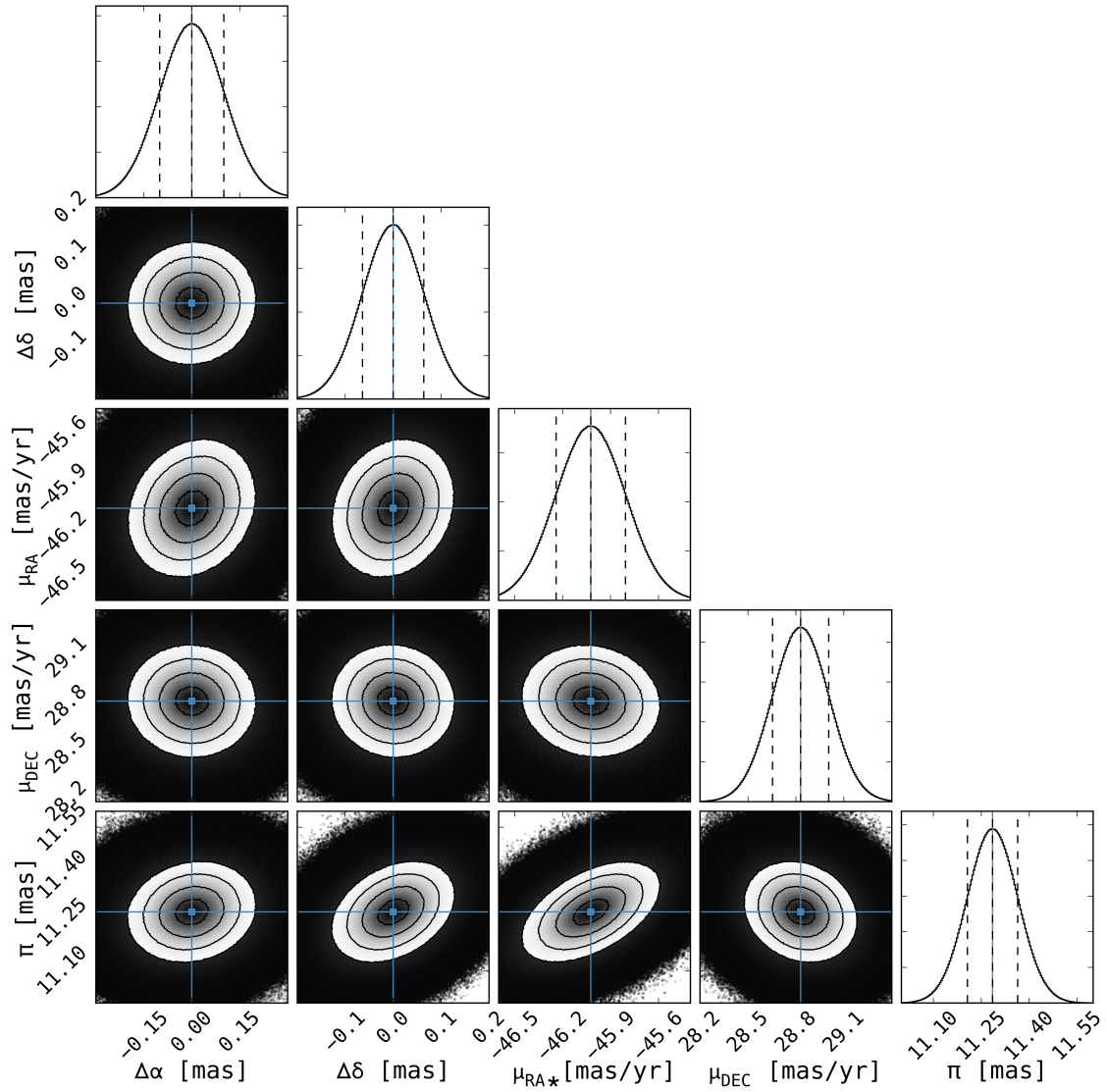

Figure 3. One- and two-dimensional projections of the posterior probability distributions of the astrometric best-fitting parameters for all EVN detections (Tab. 2) expressed through the median values and marked with the crossing blue/gray lines. The $\Delta\alpha_0$ and $\Delta\delta_0$ represents offsets relative to the position at the reference epoch t_0 = JD 2456457.5. Contours indicate 16th, 50th, and 84th percentiles of the samples in the posterior distributions also marked between vertical, dotted lines in 1-dim histograms. A single quasi-Gaussian peak of the posterior appears clearly for all parameters. The model parameters do not exhibit strong pairwise correlations, though weak, near-linear correlations between π and $\mu_{RA*} \equiv \mu^*_\alpha$, as well as between π and $\Delta\delta$ are apparent.

parameter	e-EVN (6 epochs)	e-EVN (6 epochs w.r.t. GAIA DR1)	e-EVN (4 epochs)	e-EVN+VLA (all data)
α_0	$18^{\rm hr}16^{\rm m}13.19074^{\rm s}{}^{+0.00001}_{-0.00001}$	$18^{\rm hr}16^{\rm m}13.18336^{\rm s}{}^{+0.00004}_{-0.00004}$	$18^{\rm hr}16^{\rm m}13.19074^{\rm s}{}^{+0.00001}_{-0.00001}$	$18^{\rm hr}16^{\rm m}13.19074^{\rm s}{}^{+0.00001}_{-0.00001}$
δ_0	$49^\circ52'5''.13685^{+0.00006}_{-0.00006}$	$49^\circ52'5''.18152^{+0.00028}_{-0.00028}$	$49^\circ52'5''.13684^{+0.00007}_{-0.00007}$	$49^\circ52'5''.13685^{+0.00007}_{-0.00007}$
μ^*_α [mas yr^{-1}]	$-46.02^{+0.22}_{-0.22}$	$-46.02^{+0.22}_{-0.22}$	$-46.00^{+0.19}_{-0.19}$	$-46.01^{+0.23}_{-0.24}$
μ_δ [mas yr^{-1}]	$28.83^{+0.18}_{-0.18}$	$28.83^{+0.18}_{-0.18}$	$28.83^{+0.16}_{-0.16}$	$28.83^{+0.19}_{-0.19}$
parallax π [mas]	$11.29^{+0.08}_{-0.08}$	$11.29^{+0.08}_{-0.08}$	$11.27^{+0.08}_{-0.08}$	$11.29^{+0.09}_{-0.09}$

Table 3. Parameters of the best-fitting solution for three data-sets including all e-EVN epochs in Tab. 2 (*first and second column*) at the middle-arc epoch t_0 = JD 2456457.5 and the GAIA DR1 epoch JD 2457023.5, respectively; a minimal set of four observations making it possible to determine the parallax (*the third column*) for the epoch t_0, and the set or radio-interferometric data including archival VLA measurements from NRAO database, (*right column*), also for the epoch t_0 , respectively. We note that position uncertainties for GAIA DR1 epoch (the second column) are relatively large due to parameter correlations since the initial epoch is outside the measurements time window.

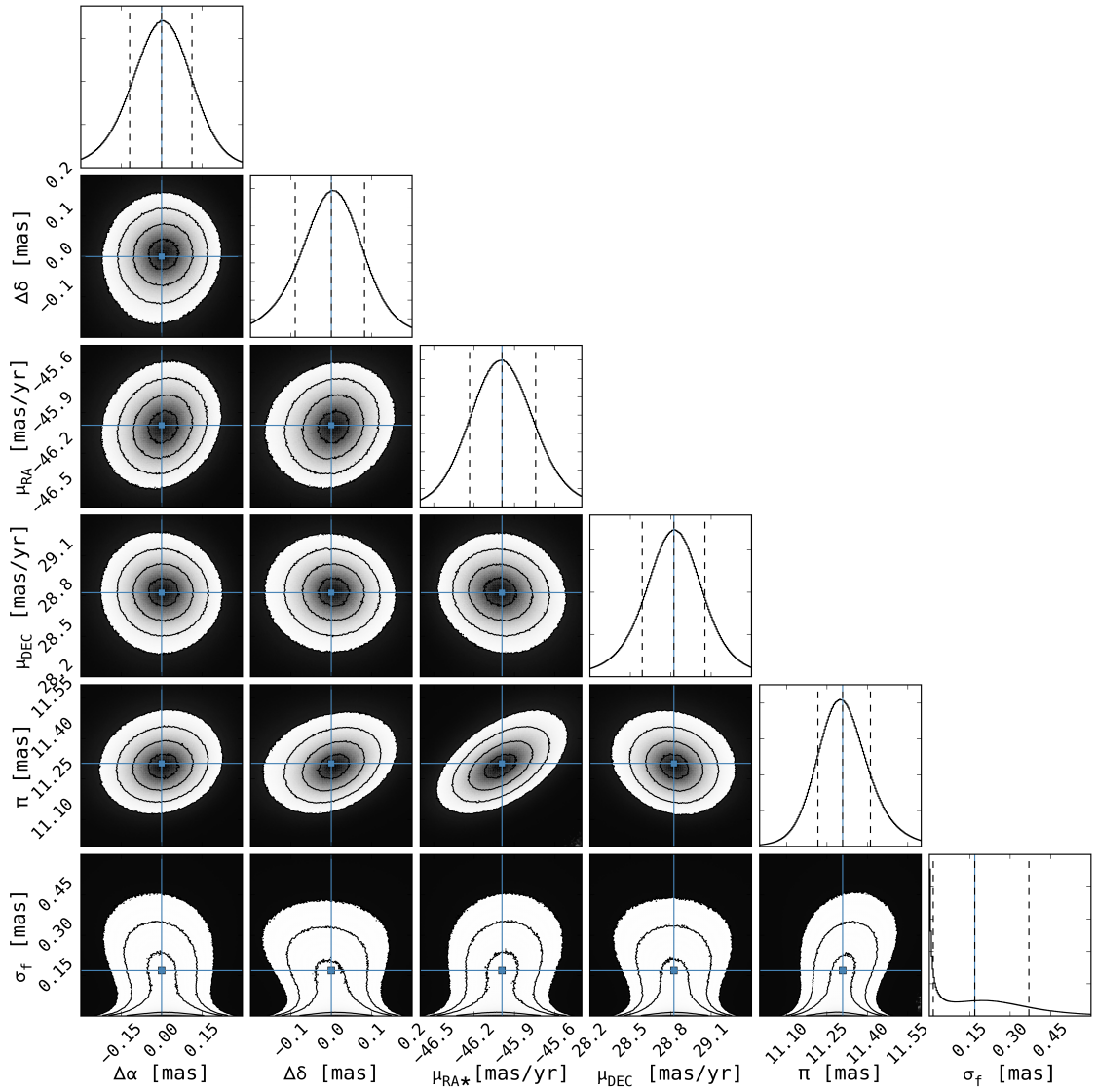

Figure 4. The same, as in Fig. 3, but for six parameters, this time including the error floor parameter (σ_f). Note that parameter ranges in both plots are the same.

tems. In order to study the physical characteristics of the quiescent emission, we estimated the brightness temperature T_B, which in the Rayleigh-Jeans regime can be approximated by

$$T_b[\mathrm{K}] \simeq 9.87 \times 10^{10} \frac{D_{100}^2 S}{r_{11}^2 \nu^2}, \quad (4)$$

(Pavelin et al. 1994), where D_{100} is the distance in units of 100 pc, S is the radio flux density in mJy, r_{11} is the radius of the emitting region in units of 10^{11} cm and ν is the frequency of the observations in units of GHz. We calculated the maximum size of the emitting region r_{11}, using estimated minimum resolvable size θ_m of an interferometer for Gaussian brightness distribution in a naturally weighted image (e.g. Kovalev et al. 2005):

$$\theta_m = \sqrt{\theta_{\mathrm{maj}} \times \theta_{\mathrm{min}}} \sqrt{\frac{4 \ln 2}{\pi} \ln\left(\frac{\mathrm{SNR}}{\mathrm{SNR}-1}\right)}, \quad (5)$$

where SNR represents the signal-to-noise ratio, θ_{min} and θ_{maj} represents the major and minor axes of the restoring beam, respectively.

AM Her appears unresolved on all our maps with SNR detections in the range ~ 7 – 20. This implies that the minimum resolvable size is equal to the upper size of the emission region, and hence the lower limit of T_b could be estimated. Our observations give r_{11}=21.7 – 36.4 (0.15 – 0.25 au), what translates to $T_b \gtrsim 0.4$ –2.4 ×10^6 K. A VLBI detection with a brightness temperature above 10^6 K is usually interpreted as a signature of non-thermal radiation, however value ~ 10^6 K do not exclude the thermal emission. Therefore, this particular estimation is ambiguous. On the other hand, the thermal radiation may come only from relatively large emission zone $\gtrsim 30\, r_{\mathrm{orb}}$ ($T_b \lesssim 10^6$ K), where $r_{\mathrm{orb}} \simeq 0.005$ au is the radius of the AM Her orbit. This radius was calculated under assumptions that the mass of the primary component is $M_{\mathrm{WD}} \simeq 0.7\,\mathrm{M}_\odot$, the secondary star mass is $M_{\mathrm{RD}} \simeq 0.3\,\mathrm{M}_\odot$, and the orbital period is $P_{\mathrm{orb}} = 3.1$ hr. The values of the parameters listed above agree with the literature data (e.g. Gänsicke et al. 2006). Such a large emission region could be considered in the case of the thermal bremsstrahlung in a stellar wind. However, using the wind analysis of Wright & Barlow

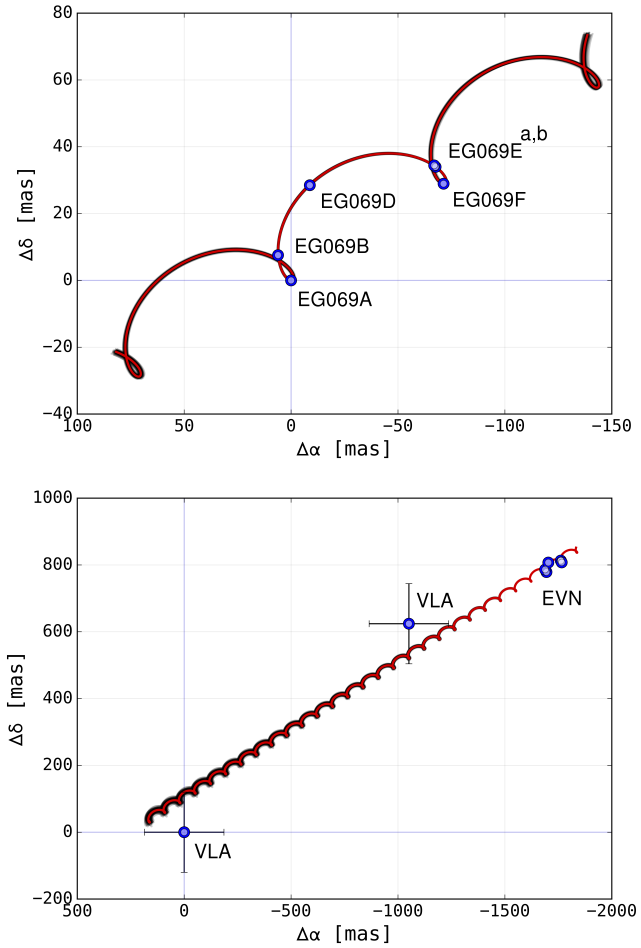

Figure 5. Sky-projected paralactic motion of the target for all e-EVN observations at epochs displayed in Tab. 2 (*top panel*), and for all radio data (*bottom panel*). Red curves are for nominal solutions in Table 3. Thin, grey curves are for 100 randomly selected samples from the MCMC-derived posterior, as illustrated in Fig. 3. Note that in all cases the synthetic curves are plotted for ±465 days, prior and beyond the first and last data epoch, respectively.

(1975), we estimate that the observed flux values could be achieved only for unrealistically high mass loss rates, i.e. for a slow wind $v_{\rm w} = 400$ km/s, required mass loss rate is $\dot{M} \sim 3 \times 10^{-8}\,{\rm M}_{\odot}$, and for a fast wind $v_w = 1500$ km/s, required mass loss rate is $\dot{M} \sim 1 \times 10^{-7}\,{\rm M}_{\odot}$. Therefore, it is unlikely that observed AM Her radio emission has thermal origin, what is in agreement with previous conclusions (e.g. Dulk et al. 1983; Mason & Gray 2007).

Curiously, the radio fluxes measured during our campaign (180 – 370 μJy) appear to be lower than those reported in the literature (so far). Moreover, our all observational epochs took place during the decreasing and the low state of the AM Her optical activity. This observational result suggests that the AM Her radio luminosity may be correlated with the mass transfer rate, which reflects in high and low states of the optical and the X-ray activity (e.g. de Martino et al. 2002). In order to study a possible correlation between the optical and the radio activity of AM Her, we collected all flux measurements at 5 & 8 GHz available in the literature, and compared them with the optical observations from AAVSO archive (Fig.7). We selected these particular radio bands, because the AM Her radio spectrum appears flat at these frequencies (Chanmugam & Dulk 1982). The high value for VLA measurement during the low optical state (15 min integration $f_{8.4\,\rm GHz} \simeq 0.63$ mJy, $m_V \simeq 15.1$, Mason & Gray 2007) is most likely due to radio flare, as during the next 15 min integration, the detected flux was $f_{8.4\,\rm GHz} \simeq 0.37$ mJy. To test a significance of a possible correlation we calculated the Pearson correlation coefficient for available data. We removed the probable flare presented in Mason & Gray (2007) from our sample and took only detections into account. The derived correlation coefficient $\sigma = 0.62$ represents moderate correlation, where p-value = 0.03 is a strong indication that the relationship is real. When the non-detections from Bastian et al. (1985) are added with the upper limits, we obtained $\sigma = 0.45$ and p-value = 0.11. The p-value indicates that we cannot reject the hypothesis that both discussed AM Her physical properties are unrelated. However, this is a small sample statistic and more data is required to make any decisive statements on this issue.

The noted difference between the archival data and the new EVN measurements of the quiescent emission can be explained in two ways. First, we consider the extended, diffused component of the AM Her radio emission, that could be resolved on VLBI scales. However, it is difficult to point out its origin. This may be a strong stellar wind from the system, but this hypothesis again needs very high mass loss rate. It also could be due to a slow expanding and decelerating shell, after the nova outburst (e.g. RS Oph, Eyres et al. 2009), although it requires quite a recent (~ 1– 10 years ago) thermonuclear runaway event in AM Her. It is clearly not the case, since from the distance about of ~ 88 pc and with a typical absolute magnitude of – $8^{\rm m}$ during the maximum (della Valle & Livio 1995), the visual optical brightness of the AM Her nova at the maximum should be $m_{max} \sim -3^{\rm m}$. This would be hardly possible to overlook nowadays.

Alternative scenario assumes that there is a correlation between the quiescent radio luminosity and the activity level of AM Her. Dulk et al. (1983) proposed, that the quiescent emission emerges through the gyrosynchrotron process caused by mildly relativistic (E~ 500 keV) electrons, which are located in the magnetosphere of the primary star. Such a correlation implies that the accretion stream provides at least partially electrons responsible for the gyrosynchrotron emission, even during very low rates of the accretion. The relationship may not be a strong one, as other effects (e.g. local magnetic activity of the secondary star) also could have impact on the quiescent emission. We prefer this scheme from two presented, because the first one generates additional problems.

Due to the quality of the e-EVN observations we were able to track evolution of the AM Her radio flux from short (~ 5 min) to long (~ months) timescales. In order to check the reliability of AM Her flux measurements we obtained fluxes for the phase calibrator J1818+5017 and the secondary calibrator J1809+5007. The fluxes for AM Her and J1809+5007 are presented on Fig.8. The scatter of J1809+5007 flux from individual scans is within ~ 10 % around the mean value, and in case of J1818+5017 in ~ 5 % around the mean with a few rare outliers. We also compared fluxes based on the upper and the lower half of the frequency band and these agree within the error with a few points with noticeable deviation. It gives us the confidence that measured AM Her fluxes are valid.

We did not detect any short-time radio outbursts, which were previously reported by Dulk et al. (1983). We observed only flux variations around an average value, which may reflect short-time changes of AM Her radio luminosity. We also checked if the radio emission is modulated with the orbital period. The phase-resolved light curve is showed on Fig.9. We used AM Her orbital ephemerids taken from Kafka et al. (2005) for the calculations. Two minima are visible in the phased radio flux, a sharp one around $\phi \sim 0.1$, and a

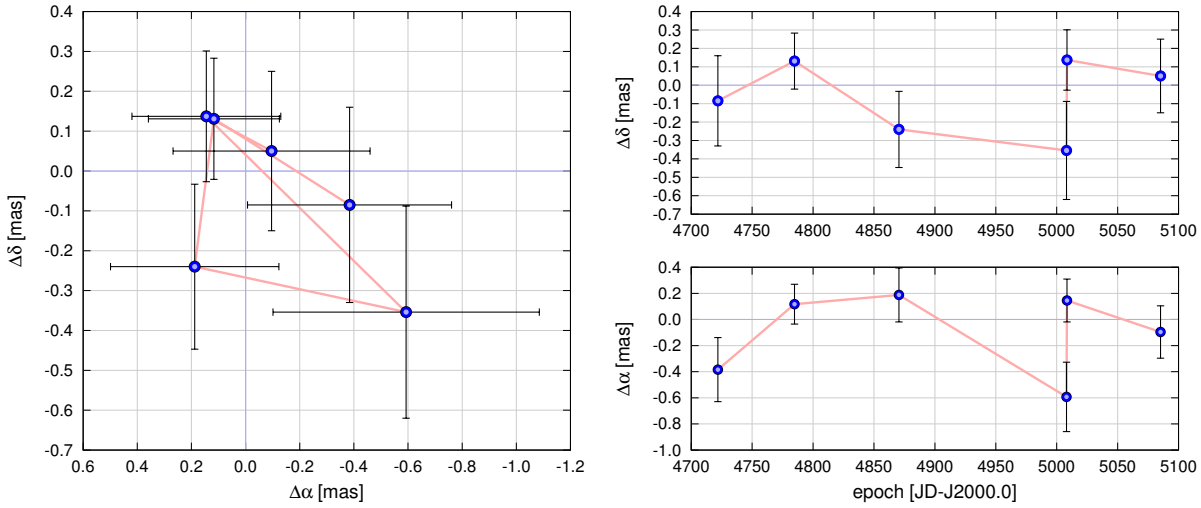

Figure 6. *Right*: Residuals to the best-fitting model in the ($\Delta\alpha$, $\Delta\delta$)-plane for all e-EVN measurements (see the model parameters in the left-hand column in Tab. 3).

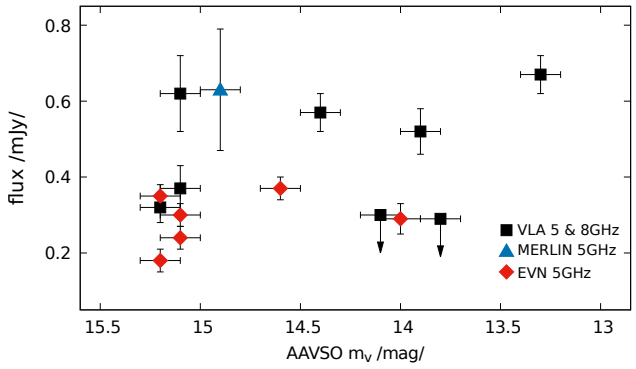

Figure 7. A comparison of the measured AM Her radio fluxes from VLA (Chanmugam & Dulk 1982; Dulk et al. 1983; Bastian et al. 1985; Mason & Gray 2007), MERLIN (Pavelin et al. 1994) and EVN (this paper) with optical observations from AAVSO data. For AAVSO data we assumed error of $0^m.1$ for 3-day average around the epoch of the e-EVN observations.

wider one with the local minimum at $\phi \sim 0.6$. We checked reliability of the phased radio light curve and repeated measurements for the upper and the lower half of the used radio band. In all cases the both mentioned minima were visible and located at the same orbital phase. This is a strong indication that the noted dependency between the orbital phase and the quiescent radio luminosity is real, however new more sensitive observations are needed to support this finding. We also investigated if presented pattern in the phase-resolved light curve could arise from a sample of random data. We calculated reduced χ^2 for the binned data relative to the mean based on all individual measurements, which gives $\chi^2 \simeq 2.6$. Next we derived χ^2 for 10000 iterations for binned data with randomized time for each single measurement. We found that a random set of data may give $\chi^2 > 2.5$, with the probability that is less than 1%. We conclude it is unlikely that the observed light curve could be a result of accidental measurements.

This observational result contradicts the proposed by Dulk et al. (1983) explanation of AM Her quiescent radio emission. The model assumes that the emission region is comparable or larger than the physical size of the binary. The new e-EVN data suggest that there is a correlation between the observed radio flux and the AM Her orbital phase. Moreover, the radio light curve is similar to observed in V471 Tau (Nicholls & Storey 1999), a pre-CV eclipsing binary with orbital period 12.51 hr. Nicholls & Storey (1999) proposed that the emission mechanism similar to RS CVn binary systems could explain observed radio properties of V471 Tau, where the gyrosynchrotron emission originates from ~ 400 keV electrons near the surface of the secondary component. This model assumes that electrons are accelerated to mildly relativistic energies, in the region where the magnetic fields of both stars are reconnecting. The accelerated electrons trapped in the K dwarf's magnetosphere are responsible for the radio emission. This interaction of fields is caused by a differential rotation of both components in V471 Tau. The radio emission arises in a wedge-like magnetic structures, which connects the acceleration region with the photosphere of the secondary component (see for details Nicholls & Storey 1999). It should be noted that the observed V471 Tau flux variations are much more prominent in comparison to AM Her. This could be just a pure geometrical effect, as in V471 Tau there is an eclipse of the radio emitting region by the K1V secondary photosphere. As the AM Her orbital inclination is relatively high ($i \simeq 50°$, e.g. Davey & Smith 1996) the probable dependency between radio flux and the orbital phase likely arises only due to different orientation of the magnetic field structures in AM Her and the line of sight. If this model is valid in the case of AM Her, one important condition should be met, the secondary red dwarf should have strong (~ kG) large scale magnetic field.

Recently, Williams et al. (2015) showed that the well-studied M9 type dwarf TVLM 513âĂŞ46546 hosts a stable, dipole magnetic field of about 3 kG at the surface. Therefore, it is plausible to assume that other low-mass red dwarfs are also able to create such strong magnetic fields. The flaring and the spectroscopic activity of the red dwarf observed during the low states of AM Her (Kafka et al. 2005, 2006) supports the idea of the strong magnetic fields on the red dwarf surface, because the flaring is a sign post of the magnetic and star-spot activity. Kafka et al. (2006) also concluded that the observed spectroscopic variations in Hα profiles are consistent with motions in large loop magnetic coronal structures on the secondary star.

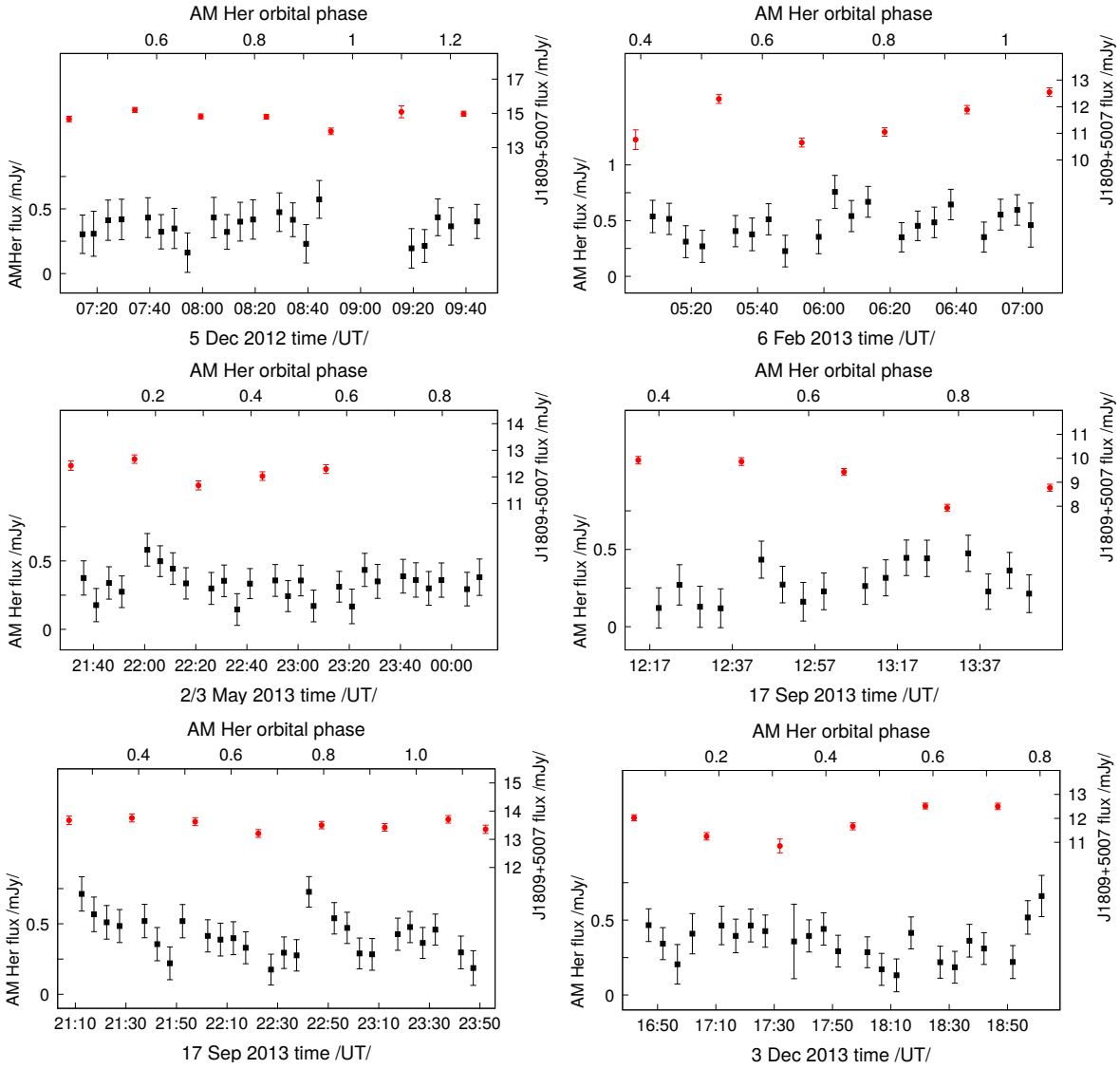

Figure 8. Variability of the radio emission obtained from our interferometric observations. Each data point represents single scan during the phase-referencing observations (• represents J1809+5007 and ■ represents AM Her, respectively) . The error bars are of length $\pm 1\sigma$.

However, the synchronous rotation of AM Her components causes problems for V471 Tau model and the process of electron acceleration should be different in AM Her. We postulate that the acceleration may originate from the interaction between red dwarf local magnetic fields frozen into transferred plasma and the white dwarf magnetosphere. The magnetic reconnection takes place near the L1 point, where the plasma accumulates during the accretion. As the local magnetic activity is very variable in the case of active red dwarfs, it may naturally explain observed variations in the quiescent radio flux in short and long timescales. This is also in agreement with the observed probable correlation between the radio luminosity and the high and low states of AM Her activity, when during the increased mass-transfer rate the electron reservoir is simply much larger ($\sim 3 \times 10^{-11}\,\mathrm{M}_\odot\,\mathrm{yr}^{-1}$ during high state and at least one order of magnitude lower during low state, de Martino et al. 1998). Observed variations in the quiescent radio flux on timescales of minutes/hours may be also interpret as changes in the mass transfer rate. Such rapid changes in the accretion are observed in the optical and X-ray domain (e.g. de Martino et al. 1998; Bonnet-Bidaud et al. 2000)

Mason & Gray (2007) discovered a second persisted radio polar AR Ursae Majoris (AR UMa), which has different physical properties than AM Her. AR UMa is a binary system with the orbital period 1.93 hr (Remillard et al. 1994). The primary white dwarf in this system has the magnetic field strength of about 230 MG (Schmidt et al. 1996), and its mass is in the range $0.91 - 1.24\,\mathrm{M}_\odot$ (Bai et al. 2016). Harrison et al. (2005) using infrared spectroscopy, estimated the spectral type of the AR UMa secondary red dwarf (M5.5 V). Mason & Gray (2007) also noted that AR UMa phased radio light curve at 8.4 GHz suggests a minimum near the orbital phase $\phi \sim 0$. If we assume that the source of the quiescent radio emission is the same in both polars, it leads to a conclusion that the emission does not depend on the physical properties of the primary white dwarf. Our findings support Mason & Gray (2007) statement, where the authors postulate that the quiescent radio emission is a sign-post of a magnetized secondary star and this distinguish AM Her and AR UMa from other polars, where no such emission

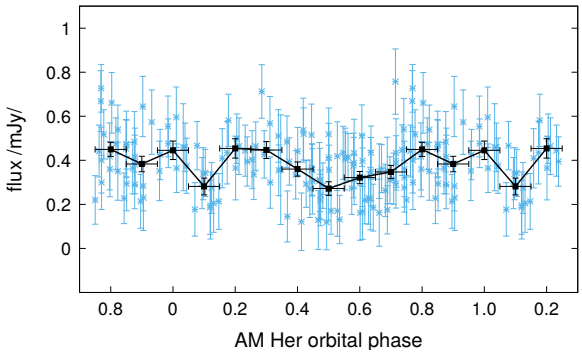

Figure 9. AM Her quiescent radio flux at 5 GHz phased with the orbital motion of the system. Cyan points represent measurements based on individual scans and black points binned values, respectively.

was detected. A more precise phased radio light curve of AR UMa of both systems in high and low states of activity would shed a new light on this puzzle.

5 CONCLUSIONS

We report our results from the recently conducted e-EVN astrometric campaign at 6 cm of AM Her. These observations were conducted in years 2012 – 2013. AM Her was detected on all six scheduled observational epochs with the quiescent radio flux in the range 0.18 – 0.37 mJy. We calculated a new AM Her astrometric model, and we determined an improved annual, absolute parallax of $\pi = 11.29 \pm 0.08$ mas with the uncertainty one order of magnitude less than in the literature. It places the AM Her almost 10 pc $\equiv$ 10% farther than predicts the most recent estimate by Thorstensen (2003). The sub-mas accuracy of the derived astrometric positions may be similar to the outcome expected from the GAIA mission, and our results could be used as an independent technique for the GAIA measurements. We demonstrated that the e-EVN makes it possible to measure the AM Her parallax with only four epochs during one year interval, still providing very low uncertainty.

We found observational evidence that the AM Her radio flux is likely modulated with the orbital phase and its behavior resembles the radio light curve noticed in V471 Tau. This behavior could be explained when the origin of AM Her radio emission is similar to proposed for V471 Tau and generally for RS CVn. We also postulate that the quiescent radio emission distinguish AM Her and AR UMa from other polars, as systems with magnetized red dwarfs. We also proposed that the correlation between the quiescent radio luminosity and the mass transfer rates (high and low states of activity) could explain noted difference between the AM Her flux based on our new EVN observations and the archival data. This may indicate that the accretion stream provides electrons, which are further accelerated and produce photons in the gyrosynchrotron process, but new sensitive radio observations of AM Her during high state and AR UMa in both activity states are needed to validate this hypothesis.

ACKNOWLEDGMENTS

We are grateful to Polish National Science Centre for the financial support (grant no. 2011/01/D/ST9/00735). The EVN is a joint facility of European, Chinese, South African, and other radio astronomy institutes funded by their national research councils. K.G. gratefully acknowledges the Poznan Supercomputing and Networking Centre (PCSS, Poland) for continuous support and computing resources through grant No. 313. This research has made use of the SIMBAD database operated at CDS, Strasbourg, France. We acknowledge with thanks the variable star observations from the AAVSO International Database contributed by observers worldwide and used in this research.

REFERENCES

Bai Y., Justham S., Liu J., Guo J., Gao Q., Gong H., 2016, ApJ, 828, 39
Bailey J., 1981, MNRAS, 197, 31
Bailey J., Ferrario L., Wickramasinghe D. T., 1991, MNRAS, 251, 37P
Bastian T. S., Dulk G. A., Chanmugam G., 1985, in Hjellming R. M., Gibson D. M., eds, Astrophysics and Space Science Library Vol. 116, Radio Stars. Reidel, Dordrecht, the Netherlands, pp 225–228
Bonnet-Bidaud J. M., et al., 2000, A&A, 354, 1003
Bunner A. N., 1978, ApJ, 220, 261
Chanmugam G., Dulk G. A., 1982, ApJ, 255, L107
Dahn C. C., et al., 1982, AJ, 87, 419
Davey S., Smith R. C., 1992, MNRAS, 257, 476
Davey S. C., Smith R. C., 1996, MNRAS, 280, 481
Dulk G. A., Bastian T. S., Chanmugam G., 1983, ApJ, 273, 249
Eyres S. P. S., et al., 2009, MNRAS, 395, 1533
Fabbiano G., Hartmann L., Raymond J., Steiner J., Branduardi-Raymont G., Matilsky T., 1981, ApJ, 243, 911
Folkner W. M., Williams J. G., Boggs D. H., Park R. S., Kuchynka P., 2014, Interplanetary Network Progress Report, 196, C1
Foreman-Mackey D., Hogg D. W., Lang D., Goodman J., 2013, PASP, 125, 306
Gänsicke B. T., Beuermann K., de Martino D., 1995, A&A, 303, 127
Gänsicke B. T., Hoard D. W., Beuermann K., Sion E. M., Szkody P., 1998, A&A, 338, 933
Gänsicke B. T., Long K. S., Barstow M. A., Hubeny I., 2006, ApJ, 639, 1039
Gawroński M. P., Goździewski K., Katarzyński K., 2017, MNRAS, 466, 4211
Greisen E. W., 2003, in Heck A., ed., Astrophysics and Space Science Library Vol. 285, Information Handling in Astronomy - Historical Vistas. Kluwer, Dordrecht, the Netherlands, p. 109, doi:10.1007/0-306-48080-8_7
Harrison T. E., Howell S. B., Szkody P., Cordova F. A., 2005, ApJ, 632, L123
Howell S. B., Ciardi D. R., Dhillon V. S., Skidmore W., 2000, ApJ, 530, 904
Kafka S., Honeycutt R. K., 2005, AJ, 130, 742
Kafka S., Honeycutt R. K., Howell S. B., Harrison T. E., 2005, AJ, 130, 2852
Kafka S., Honeycutt R. K., Howell S. B., 2006, AJ, 131, 2673
Kovalev Y. Y., et al., 2005, AJ, 130, 2473
Lindegren et al. L., 2016, A&A, 595, A4
Livio M., Pringle J. E., 1994, ApJ, 427, 956
Mason P. A., Gray C. L., 2007, ApJ, 660, 662
Melrose D. B., Dulk G. A., 1982, ApJ, 259, 844
Mouchet M., 1993, in Barstow M. A., ed., NATO Advanced Science Institutes (ASI) Series C Vol. 403, NATO Advanced Science Institutes (ASI) Series C. p. 411
Myers S. T., et al., 2003, MNRAS, 341, 1
Nicholls J., Storey M. C., 1999, ApJ, 519, 850
Pavelin P. E., Spencer R. E., Davis R. J., 1994, MNRAS, 269, 779
Ramseyer T. F., 1994, ApJ, 425, 243
Remillard R. A., Schachter J. F., Silber A. D., Slane P., 1994, ApJ, 426, 288
Schmidt G. D., Szkody P., Smith P. S., Silber A., Tovmassian G., Hoard D. W., Gänsicke B. T., de Martino D., 1996, ApJ, 473, 483
Skrutskie M. F., et al., 2006, AJ, 131, 1163
Southwell K. A., Still M. D., Connon Smith R., Martin J. S., 1995, A&A, 302, 90
Szkody P., 1978, PASP, 90, 61

Tapia S., 1977, ApJ, 212, L125
Thorstensen J. R., 2003, AJ, 126, 3017
Wickramasinghe D. T., Martin B., 1985, MNRAS, 212, 353
Wickramasinghe D. T., Bailey J., Meggitt S. M. A., Ferrario L., Hough J., Tuohy I. R., 1991, MNRAS, 251, 28
Williams P. K. G., Casewell S. L., Stark C. R., Littlefair S. P., Helling C., Berger E., 2015, ApJ, 815, 64
Wright A. E., Barlow M. J., 1975, MNRAS, 170, 41
Wu K., Chanmugam G., Shaviv G., 1995, ApJ, 455, 260
Young P., Schneider D. P., 1979, ApJ, 230, 502
Young P., Schneider D. P., 1981, ApJ, 247, 960
de Martino D., et al., 1998, A&A, 333, L31
de Martino D., Matt G., Gänsicke B. T., Silvotti R., Bonnet-Bidaud J. M., Mouchet M., 2002, A&A, 396, 213
della Valle M., Livio M., 1995, ApJ, 452, 704

This paper has been typeset from a TEX/LATEX file prepared by the author.